Characteristic electroforming behavior in $\mathrm{Pt/TiO_2/Pt}$ resistive switching cells depending on atmosphere

Doo Seok Jeong, Herbert Schroeder, Uwe Breuer, and Rainer Waser

---

Articles you may be interested in

Characteristic electroforming behavior in Pt/TiO$_2$/Pt resistive switching cells depending on atmosphere

Doo Seok Jeong,[1,a),b)] Herbert Schroeder,[1] Uwe Breuer,[2] and Rainer Waser[1]

[1]*Institute of Solid State Research and JARA—Fundamentals of Future Information Technology, Research Center Jülich, D-52425, Germany*

[2]*Central Division of Analytical Chemistry, Research Center Jülich, D-52425, Germany*

Electroforming effects on the composition, structure, and electrical resistance of Pt/TiO$_2$/Pt switching cells are investigated. The correlation between the electroforming procedure and the resulting bipolar switching behavior is discussed. The dependence of electroforming behavior on atmosphere is also identified, from which we define symmetric or asymmetric electroforming. The symmetry of electroforming is a key factor determining the resulting bipolar switching characteristics. From the experimental results we suggest a possible mechanism for electroforming in Pt/TiO$_2$/Pt in terms of the formation of oxygen gas and vacancies in the vicinity of the anode. © 2008 American Institute of Physics. [DOI: 10.1063/1.3043879]

I. INTRODUCTION

Electroforming is the initialization process for resistive switching in binary transition oxides such as TiO2,[1,2] NiO,[3] Nb$_2$O$_5$,[4] as well as perovskite-type oxides such as SrTiO$_3$ (Ref. 5) and (Ba,Sr)TiO$_3$.[6] These resistive switching oxides initially show electrically insulating behavior, with a high resistance in the gigaohm range. By applying a voltage or current to resistive switching oxides, the resistance can be degraded by many orders of magnitude. The resistance degradation induced by the applied voltage/current is termed electroforming. The electroforming process plays a very important role in resistive switching. The parameters for electroforming, including the applied voltage/current, the compliance current/voltage, and the ambient during the electroforming process, have a strong influence on the resistive switching behavior. For instance, Jeong *et al.*[2] reported that either unipolar or bipolar switching in TiO$_2$ is activated depending on the compliance current for the electroforming. In spite of the importance of electroforming, the correlation between the electroforming and the following resistive switching behavior has not yet been thoroughly investigated.

In this study, we investigate the dependence of the bipolar switching in Pt/TiO$_2$/Pt cells on the electroforming conditions by performing electroforming under various conditions such as application of different levels of voltage/current with different polarities and ambient atmospheres. A change in the composition of the electroformed switching cell is identified by conducting two-dimensional time-of-flight secondary ion mass spectroscopy (TOF-SIMS) analysis on both pristine and electroformed switching cells. The structural variation induced by the applied voltage and its relation with the resistance change is investigated using conductive atomic force microscope (C-AFM). From the experimental results we conclude a possible mechanism for electroforming and the resulting bipolar switching behavior.

II. EXPERIMENT

Pt/TiO$_2$/Pt stack switching cells were fabricated as follows. A blanket 55 nm thick TiO$_2$ thin film was deposited on a platinized Si substrate with 100 nm thick Pt layer using reactive sputtering at room temperature. From x-ray diffraction measurements and transmission electron microscope analysis the crystal structure of the TiO$_2$ film consists of small, columnar grains (diameter 10–25 nm; length=film thickness) of anatase phase, known as a stable phase of TiO$_2$ at room temperature. Circular-shaped top electrodes (TEs) of 100 μm diameter were deposited on the TiO$_2$ film using dc sputtering of Pt at room temperature. The thickness of the Pt TE was 70 nm, patterned using a shadow mask.

Voltage-controlled electroforming was performed on the as-fabricated Pt/TiO$_2$/Pt switching cells by applying a voltage to the TE and grounding the bottom electrode (BE) using a Keithley 2611 System SourceMeter. A self-made current source was used for current-controlled electroforming.

C-AFM analysis in contact mode was performed using a JEOL JSPM-4210A AFM setup. Under the applied voltage from the AFM tip a 55 nm thick TiO$_2$ film gave a very small current that was difficult to distinguish from the background noise. This is due to the insulating properties of pristine TiO$_2$. Therefore, a thinner TiO$_2$ film (10 nm) grown on 100 nm thick Pt was prepared for the C-AFM measurements.

The two-dimensional TOF-SIMS analysis was performed using a TOF-SIMS IV (ION-TOF GmbH, Muenster, Germany). The spatial resolution of the two-dimensional scan was approximately 1 μm. Depth profiles of each element were obtained by sputtering with 1 keV Cs ions.

III. EXPERIMENTAL RESULTS

A. Electroforming sequence

Applying a voltage to a switching cell can induce electroforming. In air, the electroforming into the bipolar switching state of a Pt/TiO$_2$/Pt cell is completed by several steps with alternate polarities of the electroforming voltage. At least two steps with different voltage polarities are necessary

---

FIG. 1. (a) Current-time curve of a Pt/TiO$_2$/Pt stack switching cell during the first electroforming step performed by applying a constant voltage of −8 V with a compliance of 2 mA. The first sudden degradation of the resistance occurred at about 1500 s. (b) The second electroforming occurred at +1.7 V during the voltage sweep depicted in the inset with a compliance current of 1 mA. (c) Bipolar switching curve after the second electroforming step. The inset shows the applied voltage-time cycle.
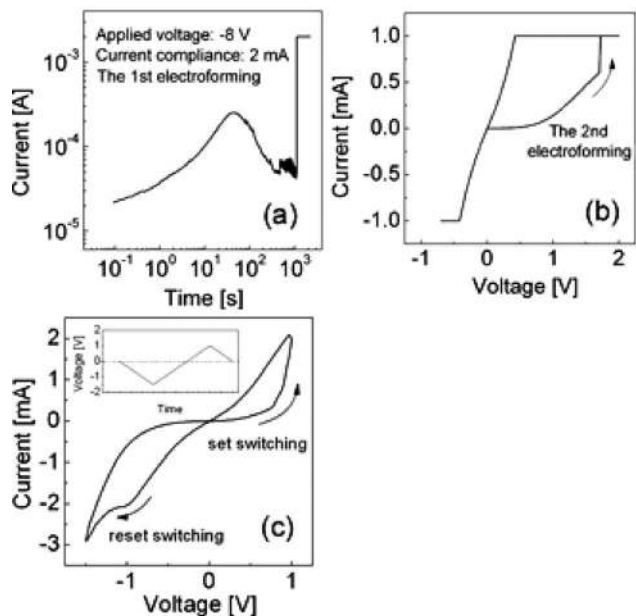

FIG. 3. (Color online) (a) Current-time curve of a Pt/TiO$_2$/Pt stack switching cell during the first electroforming step performed by applying a constant voltage of −5.5 V with a compliance of 300 μA. (b) The second electroforming step performed by applying a voltage sweep (starting with positive voltage) with a compliance current of 200 μA. The applied voltage cycle is shown in the inset of (c) with the voltage range ($V \leq 2.5$). (c) Bipolar switching curve after the second electroforming step. The inset shows the applied voltage cycle.

to complete the electroforming. The compliance current is an important parameter for voltage-controlled electroforming. Without the compliance current, the sudden decrease in the resistance of TiO$_2$ during electroforming causes a too large current, resulting in a form of hard dielectric breakdown.

Figure 1 shows an example of the electroforming procedure resulting in bipolar switching of a Pt/TiO$_2$/Pt cell. The first sudden degradation of the resistance occurred under a negative constant voltage [Fig. 1(a)] and the second degradation occurred under an opposite (positive) voltage [Fig. 1(b)]. Afterward, the stable bipolar switching shown in Fig. 1(c) could be measured. These alternate voltage applications were essential to the electroforming procedure for bipolar switching activation. The application of successive voltages with the same polarity caused electroforming into the low resistance state (LRS) of the unipolar switching mode or hard breakdown. Figure 2 illustrates the hard breakdown in-
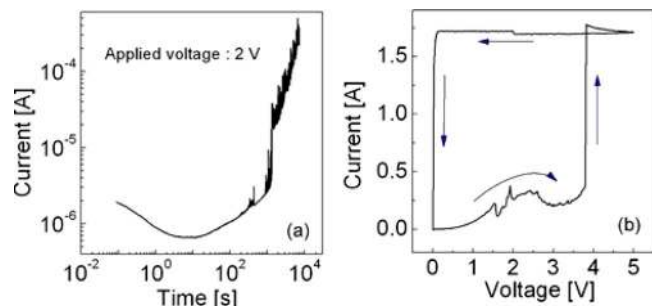

FIG. 2. (Color online) (a) The first electroforming, applying a positive constant voltage of +2 V. (b) The second electroforming, applying a positive voltage sweep, which leads to a shorted sample (breakdown).
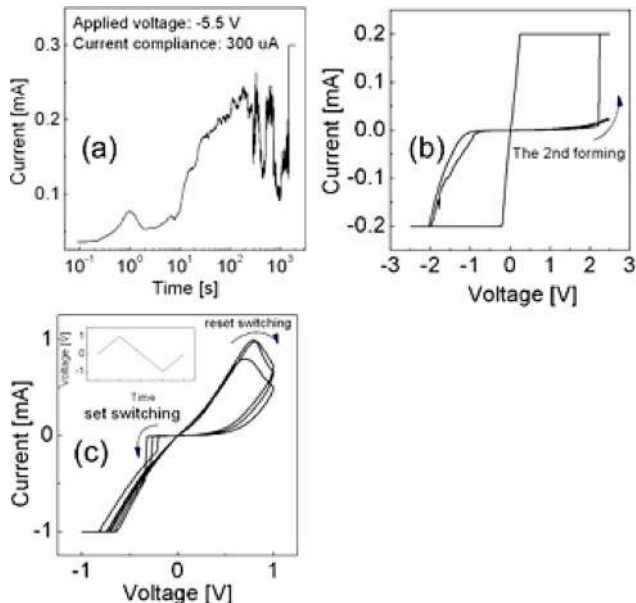
duced by the application of successive voltages with the same polarity.

A gradual increase in the compliance current for the successive electroforming steps is helpful for the activation of stable bipolar switching. In the case that the second electroforming is performed with a much higher compliance current than the first step, the electroforming often gives rise to a transition into the LRS of the unipolar switching. The completion of the electroforming could be confirmed by the observation of a gradual increase in resistance, which is often accompanied with negative differential resistance (NDR). Before the completion of the electroforming, a decrease in resistance only occurred under the alternate polarities of the applied voltage, as shown in Fig. 1. Finally, NDR took place during the voltage sweep after the last electroforming step so that the electroforming could be judged as complete. It was found that the number of the electroforming steps decreases with increasing compliance current for electroforming. However, at least two electroforming steps with the alternate polarities were necessary for the bipolar switching activation regardless of the compliance current.

The polarity of the set switching [high resistance state (HRS)→LRS] and reset switching (LRS→HRS) voltages in the bipolar switching state was determined by the first voltage cycle after completion of electroforming. Bipolar switching measurements were conducted on the as-electroformed switching cells whose electroforming behaviors are shown in Figs. 1(a), 1(b), 3(a), and 3(b). For the bipolar switching measurements two different voltage cycles were applied, plotted in the insets of Figs. 1(c) and 3(c), respectively. As shown in Fig. 1(c), the reset switching took place during the
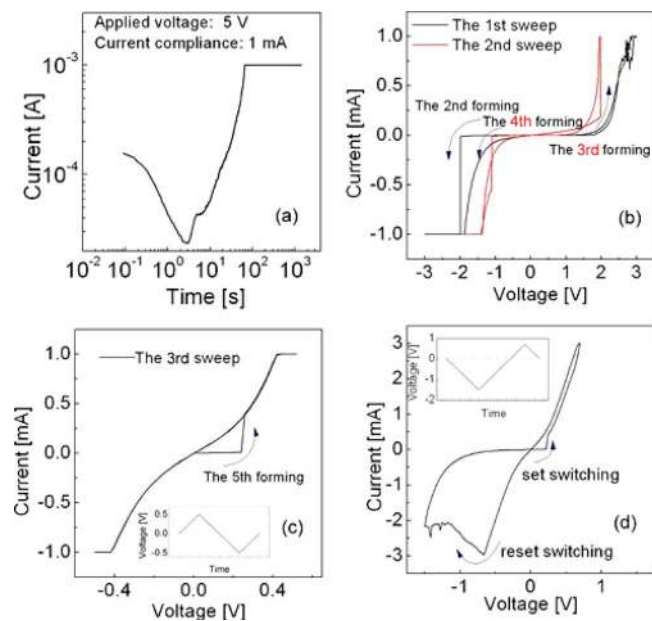
FIG. 4. (Color online) (a) Electroforming sequence of Pt/TiO$_2$/Pt. The first electroforming occurs under a constant voltage of +5 V with a compliance current of 1 mA. (b) The second to the forth electroforming occur under the voltage sweeps depicted in the inset of (c) with the voltage range, $V \leq 2$ and $V \leq 3$, respectively. (c) The fifth electroforming occurs under the voltage sweep shown in the inset. (d) Bipolar switching curve after the fifth electroforming.

FIG. 5. (Color online) Current at +0.3 V vs the absolute ratio of the currents at −0.3 and +0.3 V for Pt/TiO$_2$/Pt switching cells electroformed with compliance currents (500 μA, 1 mA, and 1.5 mA) under a constant voltage of −4 V (filled squares) and with compliance currents (500 μA and 1 mA) under a constant voltage of +2.5 V (open squares).

decrease in voltage on the negative side in the first cycle and the set switching during the increase in the positive side. However, the switching curves in Fig. 3(c) show reset and set switchings during the increase in voltage on the positive side and the decrease in the negative side, respectively. Although the electroforming procedure depicted in Figs. 3(a) and 3(b) was almost identical to that in Figs. 1(a) and 1(b), i.e., electroforming under negative voltage followed by that under positive voltage, the resulting switching curves depend on the first voltage cycle. Therefore, it is concluded that any polarity of voltage applied to as-electroformed cells leads to a reset switching during the first voltage sweep in the first cycle, and thus the different bipolar switching curves plotted in Figs. 1(a) and 3(c) are observed.

The first electroforming step cannot only occur under a negative constant voltage but also under a positive one, as exemplified in Fig. 4(a). The following additional electroforming steps performed by applying voltage sweeps are illustrated in Fig. 4(b). The second electroforming step took place under negative voltage during the first voltage cycle [the black curve in Fig. 4(b)] and the third and the fourth electroforming steps took place under the positive and the negative voltages during the second voltage cycle [the red curve in Fig. 4(b)], respectively. The electroforming procedure was similar to those shown in Figs. 1 and 3: Successive voltage application with the different polarities was always necessary. However, the degradation of the resistance shown in Fig. 4(a) is very gradual, which is different from the case of negative voltage application shown in Figs. 1(a) and 3(a).
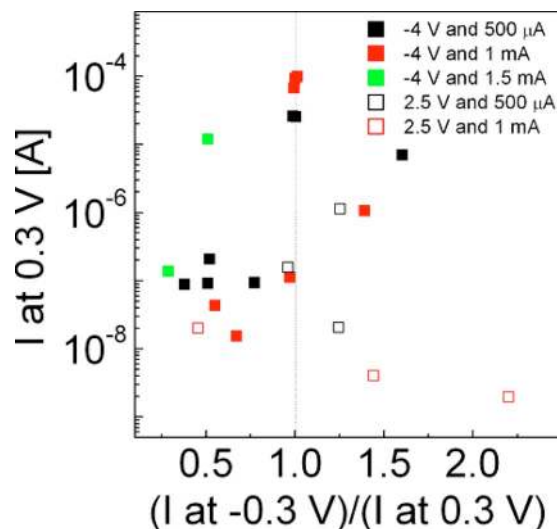
B. Dependence of electroforming on voltage and compliance current

Current-voltage (*I-V*) characteristics after the first electroforming step were influenced by electroforming parameters such as the applied voltage and the compliance current. Figure 5 shows the asymmetric *I-V* behavior and the currents at 0.3 V in switching cells electroformed with different compliance currents (500 μA, 1 mA, and 1.5 mA) under constant voltages (−4 and 2.5 V). Small voltages (0.3 and −0.3 V) were applied to the cells to avoid resistive switching. The *I-V* dependence in the electroformed state on the electroforming parameters showed large data scattering. In spite of the data scattering, a rough tendency is evident. A comparison of the currents in the cells electroformed under the negative voltage (filled squares) with those in the positively electroformed cells (open squares) identifies that currents of the same polarity as the electroforming polarity are lower than the currents measured under opposite polarity.

C. Electroforming using a current source

The electroformed state of Pt/TiO$_2$/Pt was successfully achieved using a voltage source as well as a current source. The advantage of current-controlled electroforming is that a compliance current is unnecessary. In contrast, for the voltage-controlled electroforming the compliance current is crucial to avoid the hard dielectric breakdown as mentioned earlier.

Figure 6 shows the electroforming and the bipolar switching behaviors measured using a current source. Identical to voltage-controlled electroforming, at least two electroforming steps with different polarities of applied current were needed for current-controlled electroforming. After two electroforming steps, the bipolar switching shown in Fig. 6(b) was measured with the current sweep depicted in the inset of Fig. 6(b).
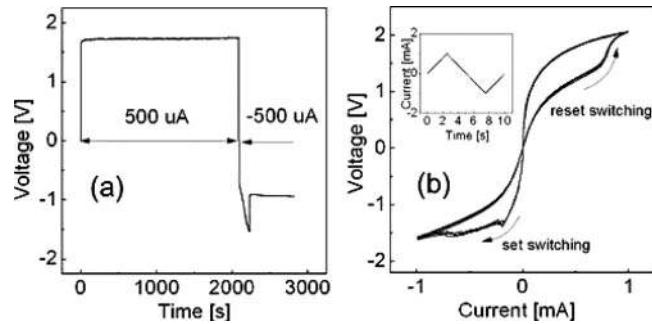
FIG. 6. (a) Electroforming of Pt/TiO$_2$/Pt performed in air by applying two successive constant currents, +500 μA in the time domain (0–2090 s) and −500 μA in the time domain (2097–2828 s). The first degradation of the resistance took place very fast in the beginning of the current application so that it could not be observed in the voltage-time curve, thus the voltage during the first constant current application seems to be a constant. The sudden drop of the voltage at 2230 s denotes an abrupt decrease in the resistance, implying that the second electroforming occurred. (b) Bipolar switching curves, following the electroforming, measured by applying the current sweep shown in the inset.

D. Electroforming in vacuum

The oxygen environment surrounding a switching cell can influence electroforming behavior as oxygen gas is considered to be involved in electroforming and the oxygen in air might react with TiO$_2$. In order to identify the effect of air on electroforming, current-controlled electroforming was performed in a vacuum chamber with a base pressure of approximately 3×10^{-5} Pa. Figure 7(a) shows voltage-time (V-t) profiles for Pt/TiO$_2$/Pt cells during electroforming in vacuum by applying two different positive constant currents
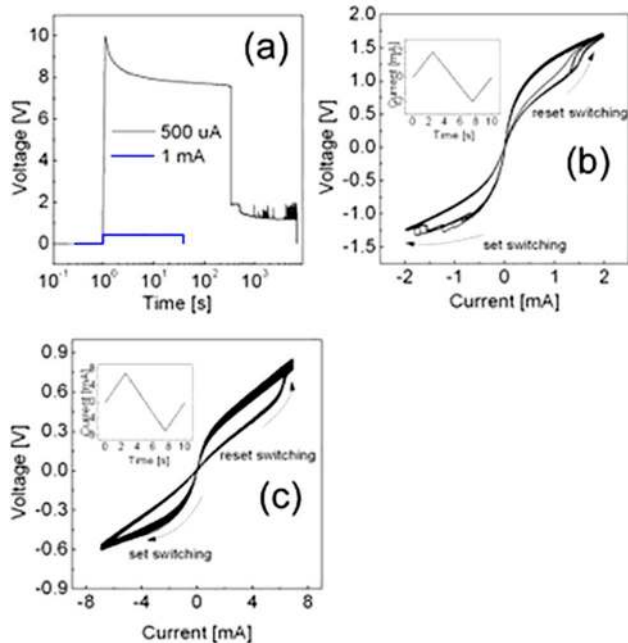

FIG. 7. (Color online) (a) Electroforming performed in vacuum by applying constant currents of 500 μA and 1 mA. The current application for electroforming started at 1 s. Under a constant current of 500 μA the small decrease in the voltage at 490 s was observed after the first abrupt drop of the voltage at 342 s. (b) Bipolar switching curves of the cell electroformed by a current of 500 μA with applying the current sweep shown in the inset. (c) Bipolar switching curves of the cell electroformed by a current of 1 mA with applying the current sweep shown in the inset.

(500 μA and 1 mA). Two discrete degradations of the resistance were induced by an applied constant current of 500 μA and then the bipolar switching [Fig. 7(b)] could be measured without additional electroforming steps under a negative-current application. Under a constant current of 1 mA the resistance degradation occurred at the onset of the current application given by a unit step function with respect to time so that a V-t curve showing the degradation could not be observed. After the very quick degradation by the higher current (1 mA) the resistance became much lower than that of the cell electroformed by the lower current (500 μA), thus the bipolar switching with lower resistance for both HRS and LRS was measured, as shown in Fig. 7(c). The resulting bipolar switching cycles are plotted in Figs. 7(b) and 7(c), respectively. The bipolar switching behavior in Fig. 7(b) is similar to that measured in air shown in Fig. 6(b). It can be seen that the stable bipolar switching state was achieved without the second electroforming step of opposite polarity, which is quite different from the observed behavior in air.

In order to identify the dependence of bipolar switching in vacuum on the polarity of the applied current, switching cells were electroformed in vacuum by applying negative currents with three different, but constant amplitudes (−100 μA, −500 μA, and −1 mA). The electroforming and the resulting bipolar switching behaviors of the cells are plotted in Fig. 8. Under a current of −100 μA the resistance underwent a single abrupt drop, as shown in Fig. 8(a). However, a second electroforming occurred during the increase in the current on the positive side, and bipolar switching could be measured, as shown in Fig. 8(b). Under the higher constant currents, either one or two degradations of the resistance took place and no additional electroforming steps were necessary for the activation of bipolar switching, which is comparable to electroforming under the positive currents shown in Fig. 7(a).

From Figs. 7 and 8 it is concluded that the applied voltage cycles for the switching measurements did not affect the polarities of the set and the reset switchings, which is different from switching measurements in air. Namely, the same voltage sweep cycle was applied for both positive- and negative-current-induced electroforming cases. Nevertheless, different switching behaviors could be achieved. Positive-current-induced electroforming resulted in set and reset switchings under negative and positive currents, respectively, whereas negative-current-induced electroforming resulted in the switchings in the opposite way, In fact, the applied voltage sweep cycle did not influence the switching behavior. For instance, a voltage sweep cycle starting with a downward sweep, which is opposite to the cycles shown in Figs. 7 and 8, resulted in the same switching behavior, as shown in Figs. 7 and 8 in vacuum (not shown in this paper).

E. Electroforming-induced compositional and structural changes

The TOF-SIMS analysis was performed on a Pt/TiO$_2$/Pt stack with a 27 nm thick TiO$_2$ layer, electroformed by applying a positive constant voltage of 5 V to the TE. Figure 9
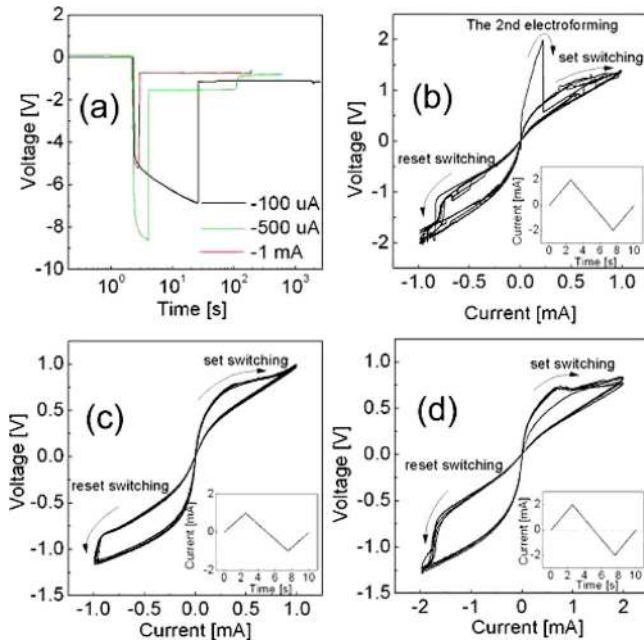
FIG. 8. (Color online) (a) Electroforming performed in vacuum by applying three different negative constant currents, −100 μA, −500 μA, and −1 mA. The current applications started at 2 s. Under a current of −100 μA the resistance underwent a single abrupt drop at 26 s. No additional decrease in the resistance occurred under the given current. Under a current of −500 μA, the resistance underwent two abrupt decreases, the first decrease at 4 s and the second one at 110 s. Afterward, no additional electroforming steps were necessary for the activation of the bipolar switching. A *V-t* curve under a current of −1 mA showed one sudden decrease in the voltage at 2.8 s. The resistance after the single decrease in the resistance was comparable to that after the two drops of the voltage in the resistance under a current of −500 μA and no additional degradations (electroforming) were necessary for the bipolar switching observation. (b) Bipolar switching curves of the cell electroformed with −100 μA. The second electroforming occurred during the increase in the current on the positive side. Eventually, the bipolar switching could be measured. Bipolar switching curves of the cell electroformed with (c) −500 μA, and (d) −1 mA.

shows the oxygen signal integrated over the depth direction at all points in the scanning area (100×100 μm^2), including the area of the circular-shaped TE with a diameter of 100 μm. Increasing brightness indicates an increase in the oxygen signal. In Fig. 9 the distribution of oxygen is found to be nonhomogeneous, indicated by a few bright spots with higher oxygen concentrations. These spots were caused by the electroforming as can be confirmed by comparison with an image of a pristine cell (not shown). The depth profiles of
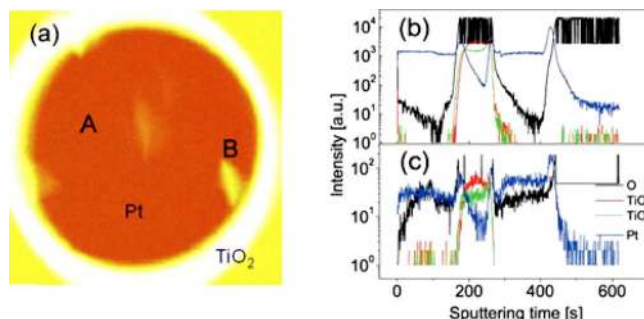

FIG. 9. (Color online) (a) Oxygen signal over the whole 100×100 μm^2 area, where the circle is the circular-shaped top electrode (100 μm diameter). (b) Depth profile at the point A in the dark area. (c) Depth profile at the bright point indicated by B.

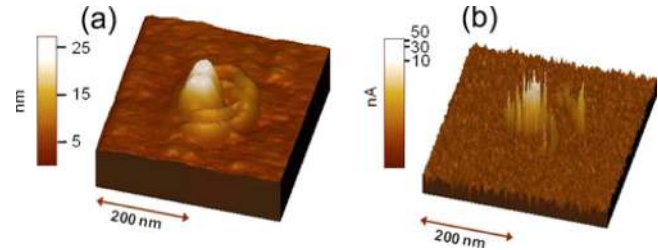FIG. 10. (Color online) (a) AFM-topography and (b) C-AFM-conductivity mapping of the same area of a TiO$_2$(10 nm)/Pt(100 nm) thin film stack.

each element or molecule (O, TiO, TiO$_2$, and Pt) at two points, one in the dark area (A) and the other in a bright spot (B), are plotted in Figs. 9(b) and 9(c), respectively. The profile in Fig. 9(c) shows oxygen incorporation into both TE and BE, whereas that in Fig. 9(b) is almost identical to that of a pristine state cell. Since the TE was the anode during electroforming, a larger amount of oxygen was incorporated into the TE than the BE. This can be identified by comparing the ratio of oxygen to platinum in the TE with that in the BE. The incorporated oxygen most probably stays at grain boundaries of Pt by forming chemisorbed states rather than platinum oxide phases (PtO$_x$).

The evolution of oxygen gas during the electroforming is expected to result in the variation of the structure of TiO$_2$ because the evolution might impose mechanical stress on the switching cell. Such a change in the microstructure of TiO$_2$ during the electroforming was confirmed by C-AFM analysis. Figure 10(a) shows the correlation between changes in the surface morphology and the conductivity of TiO$_2$. The applied negative voltage caused a huge protrusion on the surface, as shown in Fig. 10(a). The conductivity mapping after the degradation identified some parts of the protruding area having a much higher conductivity than elsewhere. However, application of a positive voltage induced no changes in topography and conductivity compared to a pristine surface.

IV. DISCUSSION

From the experimental results it was identified that the electroforming and the bipolar switching mode in TiO$_2$ are influenced by the applied voltage/current, i.e., polarity, voltage/current level, and compliance current. Furthermore, evolution of oxygen gas at the anode was identified by checking the distribution of ions over the whole volume of the electroformed Pt/TiO$_2$/Pt using TOF-SIMS, as shown in Fig. 9(b). The evolution of oxygen gas at the anode of Pt/TiO$_2$/Pt might be attributed to the formation of oxygen vacancies in TiO$_2$. The electrochemical reaction of oxygen vacancy and gas formation at the anode can be expressed in the Kröger–Vink notation as

$$O_O^\times \rightarrow V_O^{\bullet\bullet} + 2e^- + 1/2 O_2. \qquad (1)$$
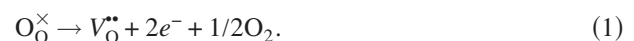
During electroforming TiO$_2$ molecules are decomposed into free oxygen ions and oxygen vacancies at the anode. Each free oxygen ion donates two electrons to the conduction band (Ti 3d band). In Fig. 9(a), the bright spots are expected to consist of TiO$_{2-n/2}$ instead of stoichiometric TiO$_2$ because of

the lack of oxygen ions in TiO$_2$. The Ti ions in the oxygen-deficient (oxygen-vacancy-enriched) regions might be reduced to fulfill the local charge neutrality, according to Ti^{4+}+$ne^-\rightarrow$Ti$^{(4-n)+}$, by capturing electrons from the cathode.[7] Therefore, the captured electrons fill the Ti 3d band. The reduced Ti ions and the oxygen vacancies can form a metallic phase, TiO$_{2-n/2}$, where n is higher than 1.5, thus creating a conduction path in the insulating TiO$_2$ matrix. Therefore, the bright spots in Fig. 9(a) might be such conduction paths. The nonhomogeneous growth of the conduction paths is most probably due to the nonuniform distribution of the electric field over the switching cell.

Consequently, bipolar switching in TiO$_2$ can be classified as anion-migration-induced switching, for which drift and diffusion of oxygen ions/vacancies result in formation and rupture of conduction paths, as it was suggested.[7] The migration of oxygen ions/vacancies determines two different resistance states, i.e., LRS and HRS. Electroforming in TiO$_2$ is therefore regarded to play a role in the formation of oxygen vacancies in TiO$_2$, leading to the formation of conduction paths. The area of the conduction paths might be a few tens μm^2 as estimated from Fig. 9(a). The estimated area is quite large compared to those judged by C-AFM measurements.[8]

Figure 10 may also demonstrate the evolution of oxygen gas at the anode. When a negative voltage was applied to the surface, oxygen gas could be evolved and accumulated at the BE (anode) causing the protrusion. However, when a positive voltage as applied, oxygen gas could be pulled out of the TiO$_2$ layer, and thus no accumulation of the oxygen gas and no consequent changes in the structure took place.

According to Eq. (1), oxygen vacancies are created in the vicinity of the anode during electroforming, inducing the decrease in resistance of TiO$_2$. Since voltages of different polarities were applied to the cells for electroforming, both TE/TiO$_2$ and TiO$_2$/BE interfaces are expected to undergo gas evolution introducing oxygen vacancies at the interfaces. The annihilation of oxygen vacancies is estimated to take place at the cathode by pushing oxygen ions incorporated in the cathode into oxygen-vacancy-enriched TiO$_{2-n/2}$. Consequently, the annihilation induces an increase in the resistance of TiO$_{2-n/2}$. It can therefore be estimated that for the bipolar switching shown in Fig. 1(c), the oxygen vacancy annihilation at the TE/TiO$_2$ interface was brought about by the first downward sweep, suggesting that the upper interface was responsible for the bipolar switching, whereas for the bipolar switching shown in Fig. 3(c), the oxygen vacancy annihilation at the TiO$_2$/BE interface was brought about by the first upward sweep so that the bottom interface controls bipolar switching.

The asymmetric distribution of oxygen vacancies might lead to the asymmetric I-V behavior as demonstrated in single crystalline TiO$_2$.[9] The interface between Pt and oxygen-vacancy-enriched TiO$_2$ (i.e., TiO$_{2-n/2}$) is not very effective in current rectification, implying the Schottky barrier height (SBH) at the interface is lower compared with the interface between Pt and stoichiometric TiO$_2$.

The degradation of the resistance under positive voltage application is much faster than under negative voltage. It took less than 100 s for the current to reach the compliance current of 1 mA [see Fig. 4(a)], whereas under negative voltage more than 1000 s were required [see Figs. 1(a) and 3(a)]. This faster degradation can possibly be attributed to easier formation of oxygen vacancies. Under positive voltage oxygen ions in the vicinity of the TE can easily escape from the switching cell leaving oxygen vacancies behind, as the TE of the cell faces the air. Under negative voltage oxygen ions are pushed into the BE and the adhesion layer (here, ZrO$_x$) below the BE so that it is relatively difficult to remove oxygen ions from the TiO$_2$ matrix. For the same reason, electroforming under the positive current (1 mA) induces higher resistance for both HRS and LRS compared to that under negative current (−1 mA), as can be identified by comparing Figs. 7(c) and 8(d).

The most obvious difference between electroforming behaviors in air and vacuum is that electroforming in air needs several steps with alternate polarities of the electroforming voltage, whereas that in vacuum needs only one step with one polarity. We term the electroforming conducted with alternate polarities as symmetric electroforming and that with one polarity as asymmetric electroforming. The cells electroformed by the symmetric electroforming procedure are estimated to undergo oxygen vacancy formation shown in Eq. (1) at both interfaces, while the asymmetric electroforming leads to asymmetric interfaces, that is, a large amount of oxygen vacancies are introduced only at one interface. Consequently, the bipolar switching following electroforming in air and vacuum involves both interfaces and one interface, respectively. Therefore, the bipolar switching following the asymmetric electroforming shown in Figs. 7(c) and 8(d) shows the polarities of the set and the reset switching depending on the polarity of the electroforming current without depending on the cycle of the applied current sweep.

For the description of the electroforming in air the chemical reaction of oxygen gas molecules in air with oxygen vacancies at the TE/TiO$_2$ interface should be taken into account. Pt is catalyst for the decomposition of gas molecules.[10] Specifically, Pt can decompose oxygen gas molecules into oxygen atoms by chemisorption of oxygen atoms at the surface according to the following reaction:[9]

$$1/2 O_{2(g)} + V_{ad} \rightarrow O_{ad}, \tag{2}$$

where V_{ad} and O_{ad} denote a vacant adatom site and an oxygen adatom, respectively. Then, the oxygen adatoms can react with oxygen vacancies according to the following reaction:

$$O_{ad} + 2e^- + V_O^{\bullet\bullet} \rightarrow O_O^{\times} + V_{ad}. \tag{3}$$
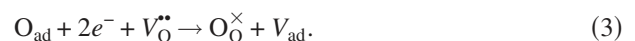
Oxygen vacancies at the TE/TiO$_x$ interface could be annihilated by virtue of oxygen gas in air according to Eqs. (2) and (3), that is, reduced Ti$^{(4-n)+}$ ions near the interface could undergo reoxidation. A mechanism for the influence of the atmosphere on the electroforming can be speculated based on the chemical reactions, Eqs. (2) and (3), for four different conditions of electroforming: applying (i) a positive voltage/current and (ii) a negative voltage/current to the TE in air and (iii) a positive voltage/current and (iv) a negative voltage/current to the TE in vacuum.

(i)   Under positive voltage/current application to the TE in air, oxygen vacancies are formed at the TE/TiO$_2$ interface according to the electrochemical reaction, Eq. (1), leading to the reduction of the SBH at the TE/TiO$_2$ interface. Therefore, the TE/TiO$_2$ interface serves as a source of oxygen vacancies. The oxygen vacancies migrate to the BE by drift and diffusion due to the applied electric field and the gradient of the oxygen vacancy concentration. The migration of the oxygen vacancies results in their accumulation at the TiO$_2$/BE interface, giving rise to the growth of an oxygen-vacancy-enriched phase (conduction path) starting from the TiO$_2$/BE interface and heading for the TE.[11] We can estimate a minimum of the oxygen vacancy concentration to appear between the source (TE/TiO$_2$) and the end of the oxygen-vacancy-enriched phase. During the growth of the conduction path from the BE, electrochemical oxidation of Ti$^{(4-n)+}$ ions in the vicinity of the TE/TiO$_2$ interface takes place, hindering the conduction path from reaching the TE. Furthermore, chemical oxidation also takes place by virtue of external oxygen, according to the chemical reactions in Eqs. (2) and (3). Consequently, the conduction path cannot connect the BE with the TE. Therefore, additional electroforming by applying a negative voltage/current is necessary to attract a large amount of oxygen vacancies to the TE/TiO$_2$ interface. The attracted oxygen vacancies can lead to the formation of a complete conduction path connecting the BE with the TE. Furthermore, the applied negative voltage will introduce a number of oxygen vacancies at the TiO$_x$/BE interface so that the SBH at the interface will be reduced as it took place at the TE/TiO$_x$ interface during the first electroforming. Sketches of the electroforming mechanism for this case are depicted in Figs. 11(a) and 11(b). In Fig. 11(a), the conducting phase is discontinuous due to the assumed minimum of the oxygen vacancy concentration.

(ii)   Under negative voltage/current application to the TE in air, a large number of oxygen vacancies are introduced at the TiO$_2$/BE interface, and thus the SBH at the interface is reduced. They drift and diffuse to the TE and accumulate at the TE/TiO$_2$ interface and then are heading for the BE. During the growth of the conduction path, the Ti$^{(4-n)+}$ ions in the vicinity of the TE/TiO$_2$ interface are electrochemically reduced due to migration of oxygen vacancies to the TE. Simultaneously, chemical oxidation occurs because of the external oxygen in air, retarding the accumulation of the oxygen vacancies at the TE/TiO$_2$ interface and also the growth of the conduction path. This can be the reason for the longer electroforming time for the negative voltage/current application compared with the positive voltage/current application as can be noticed by comparing Figs. 3 and 5 with Fig. 6. The number of oxygen vacancies accumulated at the TE/TiO$_2$ interface is not sufficient for the reduction of the SBH at the same interface because of the
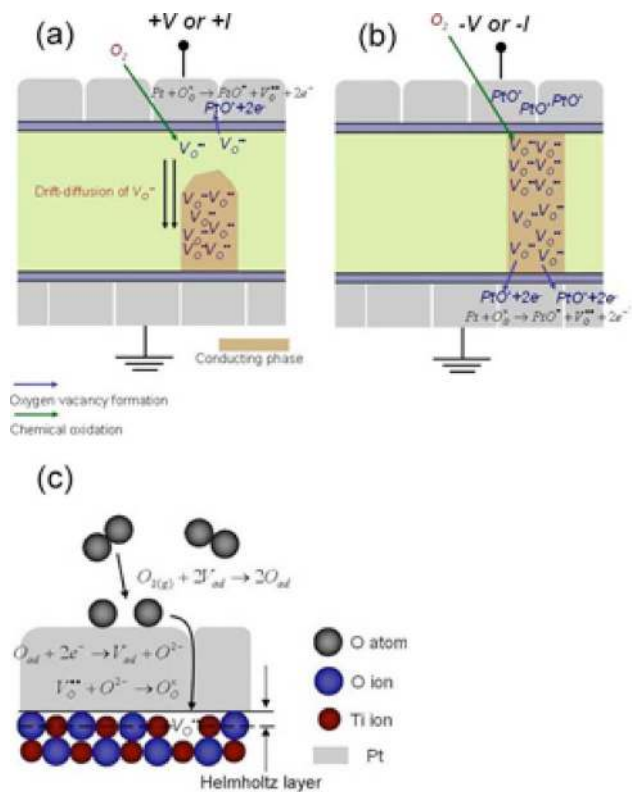

FIG. 11. (Color online) Schematic sketches of the mechanism for electroforming in air. The configuration of a conducting phase resulting from (a) the first electroforming process by applying a positive voltage/current and (b) the second electroforming by applying a negative voltage/current. TiO$_2$ between the conducting phases, shown in (a), is estimated to include more oxygen vacancies than stoichiometric TiO$_2$. PtO* denotes a chemisorbed oxygen at a Pt grain boundary. (c) The detail of the chemical reaction at the TE illustrated in (a) and (b).

chemical oxidation due to external oxygen. Therefore, additional electroforming with the positive voltage/current application is necessary for the formation of oxygen vacancies at the TE/TiO$_2$ interface to lead to the reduction in the SBH. Sketches of the electroforming mechanism for this case are depicted in Figs. 12(a) and 12(b).
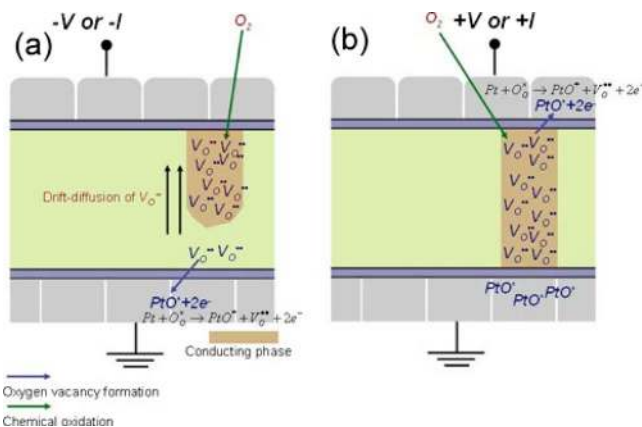

FIG. 12. (Color online) Schematic sketches of the mechanism for electroforming in air. The configuration of a conducting phase resulting from (a) the first electroforming process by applying a negative voltage/current and (b) the second electroforming by applying a positive voltage/current. The detail of the chemical oxidation is illustrated in Fig. 11(c).

(iii) For the electroforming performed in vacuum, the chemical oxidation at the TE/TiO$_2$ interface is negligible. Under positive voltage/current application to the TE, a large number of oxygen vacancies is introduced in the vicinity of the TE/TiO$_2$ interface. The introduced oxygen vacancies drift and diffuse to the BE so that they accumulate at the TiO$_2$/BE interface, resulting in the SBH reduction. Conduction paths grown from the TiO$_2$/BE interface can reach the TE since chemical oxidation can be ruled out. Therefore, electroforming can be completed by single positive voltage/current application.

(iv) In case of negative voltage/current application to the TE in vacuum, the oxygen vacancies formed at the TiO$_2$/BE interface drift and diffuse to the TE and can accumulate at the TE/TiO$_2$ interface. Therefore, conduction paths grow from the TE/TiO$_2$ interface and reach the BE without an additional electroforming step.

Considering a low diffusivity and mobility of oxygen vacancies in the TiO$_2$ matrix, it can be estimated that the accumulation of oxygen vacancies at the cathode and the growth of the conduction paths from the cathode are time-consuming phenomena. The diffusion coefficient of oxygen vacancies (D_V) in TiO$_2$ at relatively low temperatures (<1000 °C) has not been clarified yet. Nevertheless, D_V can be roughly evaluated from a conductivity change due to the chemical oxidation of reduced TiO$_{2-\delta}$ in the temperature regime (200–325 °C).[12] Experimental results in Ref. 12 identify that $K_p = D_V \Delta \delta$ is given by $K_P = 2 \times 10^{-12} e^{-0.69/kT}$ in the given temperature regime. $\Delta \delta$ denotes the difference in the stoichiometry of TiO$_{2-\delta}$ between the surface of TiO$_2$ film facing the oxygen atmosphere and the oxygen-deficient TiO$_{2-\delta}$ bulk region. Under the assumption that the TiO$_{2-\delta}$ film does not consist of second phases such as the Magnelli phase, $\Delta \delta$ would be 0.008 at most.[13] Therefore, we obtain $D_V \sim 6.4 \times 10^{-18}$ cm^2/s at room temperature. Using this D_V and the Nernst–Einstein equation, the mobility of the oxygen vacancies can be calculated to be 2.5×10^{-16} cm^2/V s. From this mobility, a time approximately necessary for the migration of the oxygen vacancies from the anode to the cathode can be estimated to be 15000 s at an applied voltage of −8 V. As shown in Fig. 1(a), the calculated time is about one order of magnitude higher than the measurement result. This difference might be attributed to either the approximated calculation or the underestimated D_V. The diffusion coefficient of grain boundary diffusion is much higher than bulk diffusion.[14] As a matter of fact, the TiO$_2$ films in this study are composed of small columns whose diameter is about 15 nm so that it can be assumed that grain boundary diffusion is dominant.

The mechanism of the chemical oxidation due to the external oxygen needs more elaboration. Electroformed cells are found to stay in the electroformed state for a few weeks in air without the applied voltage/current. It can therefore be guessed that chemical oxidation during electroforming might be differentiated from that in the static state in which no external voltage/current exists. One should quantitatively elucidate the effect of the chemical oxidation on the electroforming, in which the formation, the annihilation, and the migration of oxygen vacancies simultaneously take place in order to clarify this important assumption.

V. CONCLUSIONS

At least two electroforming steps with alternate polarities of the applied voltage/current (symmetric electroforming) were necessary for the activation into the bipolar switching mode of Pt/TiO$_2$/Pt cells in air, whereas the electroforming performed in vacuum could be completed by a single electroforming step with one polarity (asymmetric electroforming). The evolution of oxygen gas at the anode during electroforming, was confirmed by the TOF-SIMS measurements that could explain the C-AFM measurements. Furthermore, from the nonuniform distribution of oxygen ions incorporated into the anode, identified by the TOF-SIMS analysis, it can be assumed that conduction paths are inhomogeneously distributed and composed of oxygen-deficient phases formed during the electroforming.

The chemical oxidation, taking place in the vicinity of the TE due to the external oxygen gas in air, is assumed to retard the accumulation of oxygen vacancies at the cathode (=TE) so that additional electroforming with opposite polarity should be performed to introduce oxygen vacancies at the new anode (=TE, which was the cathode during the previous electroforming).

[1] B. J. Choi, D. S. Jeong, S. K. Kim, C. Rohde, S. Choi, J. H. Oh, H. J. Kim, C. S. Hwang, K. Szot, R. Waser, B. Reichenberg, and S. Tiedke, J. Appl. Phys. **98**, 033715 (2005).

[2] D. S. Jeong, H. Schroeder, and R. Waser, Electrochem. Solid-State Lett. **10**, G51 (2007).

[3] J. F. Gibbons and W. E. Beadle, Solid-State Electron. **7**, 785 (1964).

[4] T. W. Hickmott, J. Vac. Sci. Technol. **6**, 828 (1969).

[5] K. Szot, W. Speier, G. Bihlmayer, and R. Waser, Nature Mater. **5**, 312 (2006).

[6] R. Oligschlaeger, R. Waser, R. Meyer, S. Karthäuser, and R. Dittmann, Appl. Phys. Lett. **88**, 042901 (2006).

[7] R. Waser and M. Aono, Nature Mater. **6**, 833 (2007).

[8] K. M. Kim, B. J. Choi, B. W. Koo, S. Choi, D. S. Jeong, and C. S. Hwang, Electrochem. Solid-State Lett. **9**, G343 (2006).

[9] J. R. Jameson, Y. Fukuzumi, Z. Wang, and P. Griffin, Appl. Phys. Lett. **91**, 112101 (2007).

[10] W. X. Li, L. Österlund, E. K. Vestergaard, R. T. Vang, J. Matthiesen, T. M. Pedersen, E. Lægsgaard, B. Hammer, and F. Besenbacher, Phys. Rev. Lett. **93**, 146104 (2004).

[11] R. Waser, T. Baiatu, and K. H. Härdtl, Ferroelectrics **109**, 89 (1990).

[12] A. Rothschild, Y. Komem, and F. Cosandey, J. Electrochem. Soc. **148**, H85 (2001).

[13] P. Kofstad, *Nonstoichiometry, Diffusion and Electrical Conductivity in Binary Metal Oxides* (Wiley, New York, 1972).

[14] G. Gottstein, *Physical Foundations of Materials Science* (Springer, Berlin, 2004).